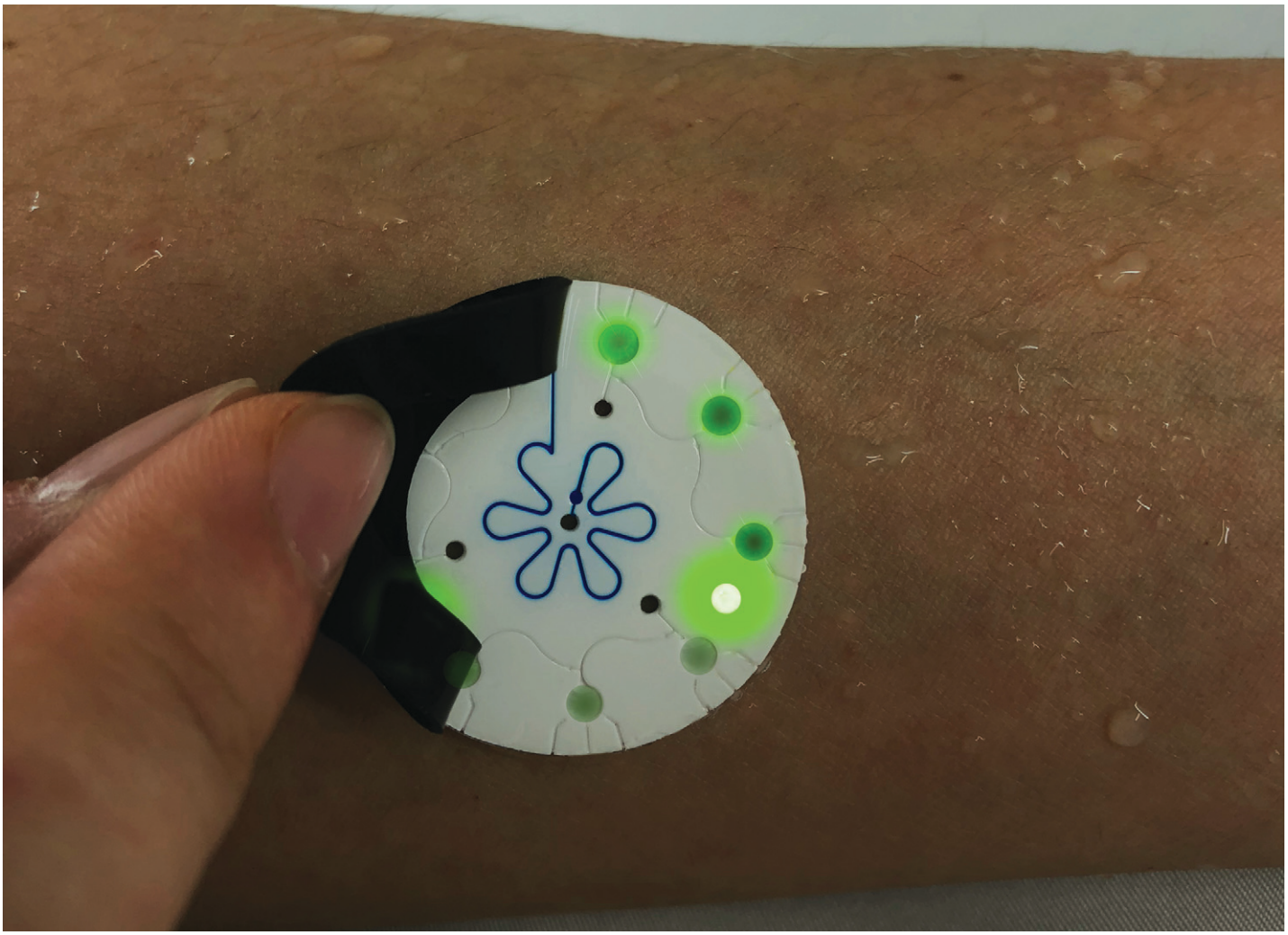

Featuring work from Professor John A. Rogers, Northwestern University, United States.

A fluorometric skin-interfaced microfluidic device and smartphone imaging module for *in situ* quantitative analysis of sweat chemistry

A skin-interfaced, fluorometric microfluidic system paired with a smartphone-based imaging module allows time-sequential sweat collection sampling in micro reservoirs and in situ quantitative analysis of biomarkers in sweat with high accuracy.

As featured in:

See Yurina Sekine, John A. Rogers *et al.*, *Lab Chip*, 2018, **18**, 2178.

ROYAL SOCIETY OF CHEMISTRY

rsc.li/loc

Registered charity number: 207890

Lab on a Chip

PAPER

Cite this: *Lab Chip*, 2018, **18**, 2178

A fluorometric skin-interfaced microfluidic device and smartphone imaging module for *in situ* quantitative analysis of sweat chemistry†

Yurina Sekine, *[a] Sung Bong Kim,[b] Yi Zhang,[cd] Amay J. Bandodkar,[cd] Shuai Xu,[de] Jungil Choi,[cd] Masahiro Irie,[f] Tyler R. Ray,[cd] Punit Kohli,[g] Naofumi Kozai,[h] Tsuyoshi Sugita,[h] Yixin Wu,[c] KunHyuck Lee,[c] Kyu-Tae Lee,[i] Roozbeh Ghaffari[dj] and John A. Rogers*[bcdejklmn]

Received 26th May 2018,
Accepted 25th June 2018

DOI: 10.1039/c8lc00530c

rsc.li/loc

The rich composition of solutes and metabolites in sweat and its relative ease of collection upon excretion from skin pores make this class of biofluid an attractive candidate for point of care analysis. Wearable technologies that combine electrochemical sensors with conventional or emerging semiconductor device technologies offer valuable capabilities in sweat sensing, but they are limited to assays that support amperometric, potentiometric, and colorimetric analyses. Here, we present a complementary approach that exploits fluorometric sensing modalities integrated into a soft, skin-interfaced microfluidic system which, when paired with a simple smartphone-based imaging module, allows for *in situ* measurement of important biomarkers in sweat. A network array of microchannels and a collection of microreservoirs pre-filled with fluorescent probes that selectively react with target analytes in sweat (*e.g.* probes), enable quantitative, rapid analysis. Field studies on human subjects demonstrate the ability to measure the concentrations of chloride, sodium and zinc in sweat, with accuracy that matches that of conventional laboratory techniques. The results highlight the versatility of advanced fluorescent-based imaging modalities in body-worn sweat microfluidics platforms, and they suggest some practical potential for these ideas.

Introduction

The skin contains over two million eccrine glands distributed across the surface of the human body to regulate core temperature.[1–5] These sweat glands excrete water and a rich composition of electrolytes (chloride, sodium, and potassium), metals (iron, magnesium, and zinc), metabolites (lactate, glucose, urea, and creatinine), proteins, and exogenous chemicals (alcohol and drugs).[6,7] Studies demonstrate that the concentrations of these and other biomarkers in sweat can provide important insights into nutrition and health, as well as cognitive and physical performance, thus making this class of biofluid attractive across a broad range of applications in diagnostics, sports performance, and ambulatory monitoring.[8–11]

A key challenge in the use of sweat for such purposes is in the clean capture and collection of small quantities of sweat as it emerges from the eccrine glands, and before it is contaminated by oils, residual dirt or other chemicals on the surrounding skin and/or in the external environment.

[a] *Materials Sciences Research Center, Japan Atomic Energy Agency, Tokai, Ibaraki, 319-1195, Japan. E-mail: sekine.yurina@jaea.go.jp*
[b] *Department of Materials Science and Engineering, and Frederick Seitz Materials Research Laboratory, University of Illinois at Urbana-Champaign, Urbana, IL 61801, USA*
[c] *Department of Materials Science and Engineering, Northwestern University, Evanston, IL 60208, USA. E-mail: jrogers@northwestern.edu*
[d] *Center for Bio-Integrated Electronics, Simpson Querrey Institute for Bio-Nanotechnology, Northwestern University, Evanston, IL 60208, USA*
[e] *Department of Dermatology, Feinberg School of Medicine Center for Bio-Integrated Electronics, Northwestern University, Chicago, IL 60211, USA*
[f] *Department of Mechanical Engineering, Keio University, Yokohama, Kanagawa, 223-8522, Japan*
[g] *Department of Chemistry and Biochemistry, Southern Illinois University, Carbondale, IL 62901, USA*
[h] *Advanced Science Research Center, Japan Atomic Energy Agency, Tokai, Ibaraki, 319-1195, Japan*
[i] *Department of Physics, Inha University, Incheon, 22212, Republic of Korea*
[j] *Department of Chemistry and Biomedical Engineering, Northwestern University, Evanston, IL 60208, USA*
[k] *Department of Electrical Engineering and Computer Science, Northwestern University, Evanston, IL 60208, USA*
[l] *Department of Neurological Surgery, Northwestern University, Evanston, IL 60208, USA*
[m] *Department of Chemistry, Northwestern University, Evanston, IL 60208, USA*
[n] *Department of Mechanical Engineering, Northwestern University, Evanston, IL 60208, USA*

† Electronic supplementary information (ESI) available. See DOI: 10.1039/c8lc00530c

Traditionally, analysis of sweat volume and composition relies on extraction of sweat from absorbent pads pressed against the skin.[12,13] This strategy requires sample storage, centrifugation, and then insertion into benchtop equipment for liquid chromatography, chloridometry, mass spectrometry, or other types of analysis. Such approaches are susceptible to contaminants that can be introduced in various stages of this process and they also require systems for handling the sweat, along with benchtop equipment and supporting laboratory facilities for measurement. Recently reported wearable devices for sweat analysis provide *in situ* analysis capabilities that avoid some of these limitations, but they do not include microfluidic features for capture, storage and/or routing of sweat, for measuring sweat loss or rate, or for chemical manipulations and pre-conditioning needed for certain types of measurements.[14–18]

The development of advanced, soft microfluidics devices addresses many of these limitations[15,19–21] The device designs in such cases involve multi-layer stacks that include a skin adhesive interface, localized inlet ports, an integrated microfluidic substrate with microchannels, valves and microreservoirs, and a top layer that seals the system and serves as a mounting location for graphics overlays to facilitate visual or image-based readout. The systems are thin, flexible and capable of elastically accommodating large strain deformations, thereby allowing conformal, water-tight integration with the curved surfaces of the skin without constraint on natural motions. This unique type of platform facilitates collection of sweat from the surface of the skin through naturally occurring release processes *via* pores that connect to eccrine glands, from single or multiple locations at nearly any region of the body, with wide-ranging design options in size, microfluidic layouts and form factor.

The ability to extract sweat in this manner for laboratory evaluation is powerful, but it is limited to post-collection analysis. In some cases, real-time capabilities in monitoring of sweat biomarkers are important. Colorimetric assays provide a powerful option that obviates the need for electrochemical measurements, along with the associated power supplies and data communication hardware.[22–24] Recent reports describe means for using colorimetric chemistry in such wearable, microfluidic sweat sensing systems to perform quantitative measurements of chloride, lactate, glucose and pH across physiologically relevant ranges.[15,19–21,25] These assays can be performed semi-quantitatively by eye, *via* comparisons against color calibration markings printed on the top layer of the devices, or quantitatively through digital analysis of images captured with a smartphone. A main drawback is that colorimetric assays exist only for a relatively narrow range of biomarkers.

A fluorescence-based analysis of sweat could represent a complementary approach. Here, the amounts of target solutes or metabolites follow from measurements of fluorescence emitted by chemical probes, using a light source for excitation and a photodetector for quantifying the emission. A range of such probes are available for quantitative measurements of biomarker concentrations with high sensitivity from biological samples that contain small amounts of target biomolecules or pathogens, both *in vivo* and *in vitro*. Furthermore, recent work on smartphone optics suggest that *in vitro* fluorescence-based diagnostics and analysis can be performed at low-cost in the field.[26–30]

Here, we adapt and extend these ideas to allow their use in fluorometric approaches to sensing of sweat captured in wearable microfluidic devices *via* smartphone-based fluorescence-imaging modules. The specific results focus on determination of sweat chloride, sodium, and zinc *in situ*, with high sensitivity, wherein microliter quantities of sweat flow through microchannels and valves into microreservoirs that contain fluorometric probes. Sweat chloride and sodium have the most established clinical relevance, and their concentrations have been used as diagnostics for cystic fibrosis.[9] Furthermore, the concentration of zinc in sweat can serve as an indicator of zinc deficiency.[31] Reaction of the probes in microreservoirs with specific ions (chloride, sodium, and zinc) leads to changes in the intensity of fluorescence excited and detected using a smartphone fitted with an optics module. The concentrations determined using these platforms in the field on human subjects match those obtained using traditional laboratory methods.

Results and discussions

Skin-mounted, fluorometric microfluidic device design

Fig. 1 illustrates the key design features of the fluorometric sweat sensing devices introduced here. The multilayer stack includes three components: an ultrathin, skin-compatible adhesive layer with openings to localized regions of the skin, a platform of microfluidic channels and valve structures that route sweat excreted from these regions to microreservoirs with fluorometric reagents, and a detachable light-shielding layer to prevent exposure of these reagents to light prior to the readout process. The adhesive membrane enables water-tight, biocompatible attachment to the skin. Openings in the adhesive define sweat collection zones (~3 mm in diameter), approximately 110 cm^{-2} sweat glands on the upper arm.[5] These zones interface to small inlet openings at the base of the microfluidic layer as a fluid path from the skin to the microchannels and microreservoirs. Positive pressure generated by natural sweat excretion mechanisms[32] drive the flow of sweat through the inlets and into the microfluidic system (Fig. 1a).

The geometries and dimensions of the microfluidic channels, valves and microreservoirs are sufficiently large to support largely unimpeded flow of sweat across the physiologically relevant range of sweat rates. The microfluidic channels lead to microreservoir regions that contain fluorescent assays tailored for chloride, sodium, and zinc. Sweat that flows through the microchannels eventually reaches the microreservoirs and mixes with the assay chemicals (Fig. 1b). The three microreservoirs in this representative device connect by curved channels and capillary bursting valves designed to

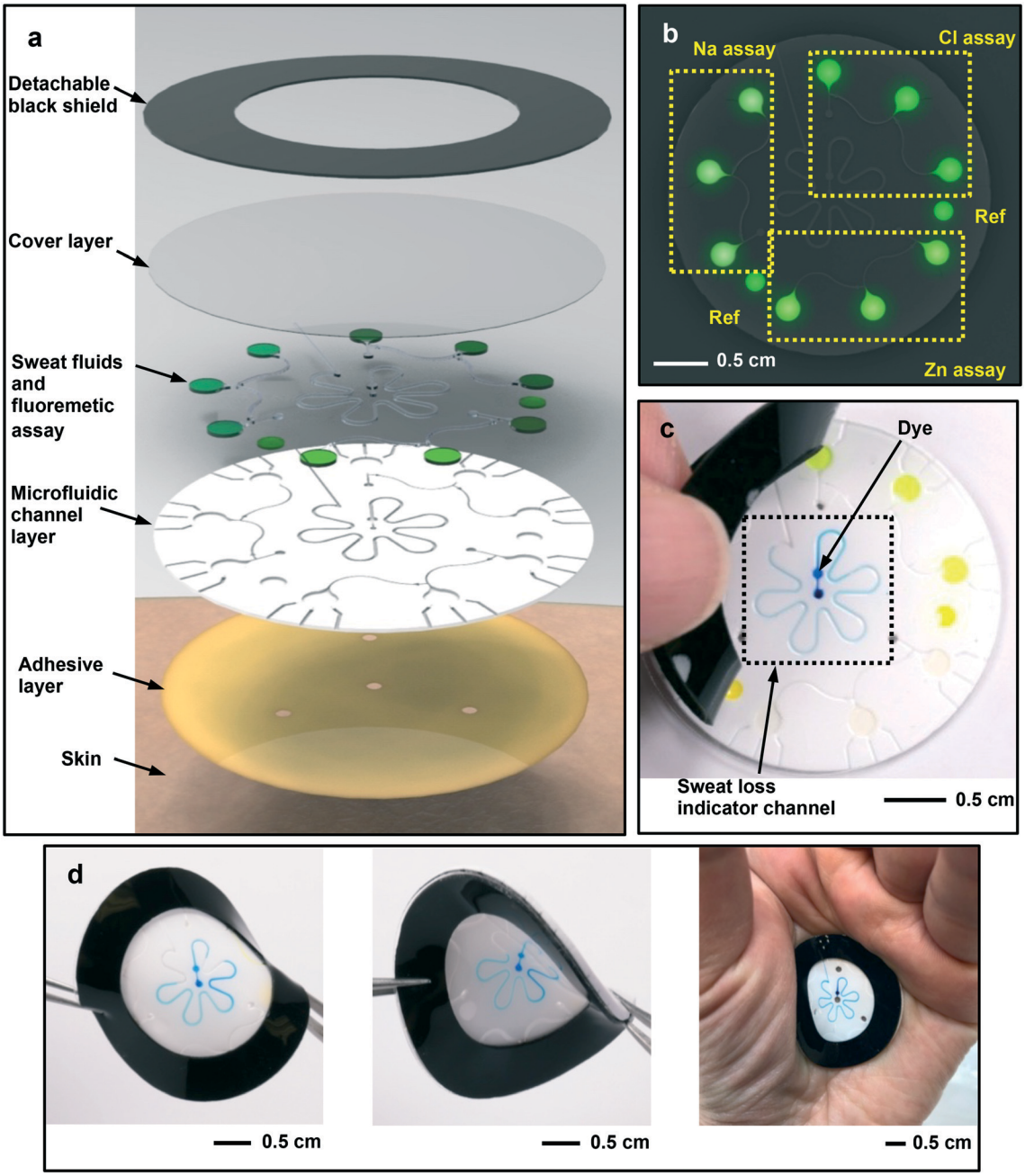

Fig. 1 Schematic illustration and digital images of a skin-interfaced microfluidic device for sensing the concentrations of chloride, sodium, and zinc in sweat by fluorometric methods. (a) Schematic exploded view illustration of the microfluidic platform for collection, capture and storage of sweat with *in situ* capabilities for fluorescence assays. (b) Image illustrating fluorescence signals associated with chemical probes designed to respond to chloride, sodium, and zinc embedded in a device under excitation light. Image of (c) peeling the detachable black shield away from the microfluidic device and (d) mechanical flexing: forward twisting (left) and backward twisting (center), and on the palm (right).

allow fluid to pass only at sufficiently high pressures (Fig. S1(a–c)†).[20] These valves provide time-sequential sweat collection sampling (Fig. S1d†) of ~2 μL in each reservoir, for a total volume of 8.1 μL. The two round reservoirs located between the assay systems serve as fluorescence reference markers that consist of an ionic liquid of known concentration mixed with a fluorescent dye. A thin ring of a black silicone attaches to the top surface of the device to prevent photobleaching of the fluorescence probes. The low elastic modulus (~1 MPa)[33,34] and naturally adherent surfaces of the silicone materials allow this layer to be detached and reapplied easily and reversibly (Fig. 1c).

In addition to fluorescence-based analysis of sweat biomarkers, the flower-shaped microchannel in the center of the device allows measurements of total sweat loss and rate. Sweat that flows through this microchannel dissolves a water-soluble dye located near the inlet, thereby creating a highly visible colored liquid front that moves along the

microchannel (Fig. S1e†). The amount of sweat that fills this channel system has a known volume, determined by the extent of filling from glands with access to the corresponding inlet. This volume of local sweat loss can be correlated to total body loss *via* a calibration factor.[15]

The low effective modulus and high elasticity (up to ~200%) of the microfluidic substrate allows the device to achieve intimate, water-tight mechanical coupling to the surface of the skin. Fig. 1d shows deformations of a representative device on the skin, in response to bending and twisting. The device elastically accommodates these forces, thereby allowing attachment to nearly any region of the human body for sweat collection and analysis.

A smartphone-based optical setup for fluorometric imaging

An optical module with integrated filters attaches to the lens and imager of a smartphone to facilitate routine, rapid measurements in the field. Fig. 2a illustrates the key features of this module and its coupling to the smartphone. A dark shielded box with excitation and emission filters enables capture of fluorescence images using standard camera functions

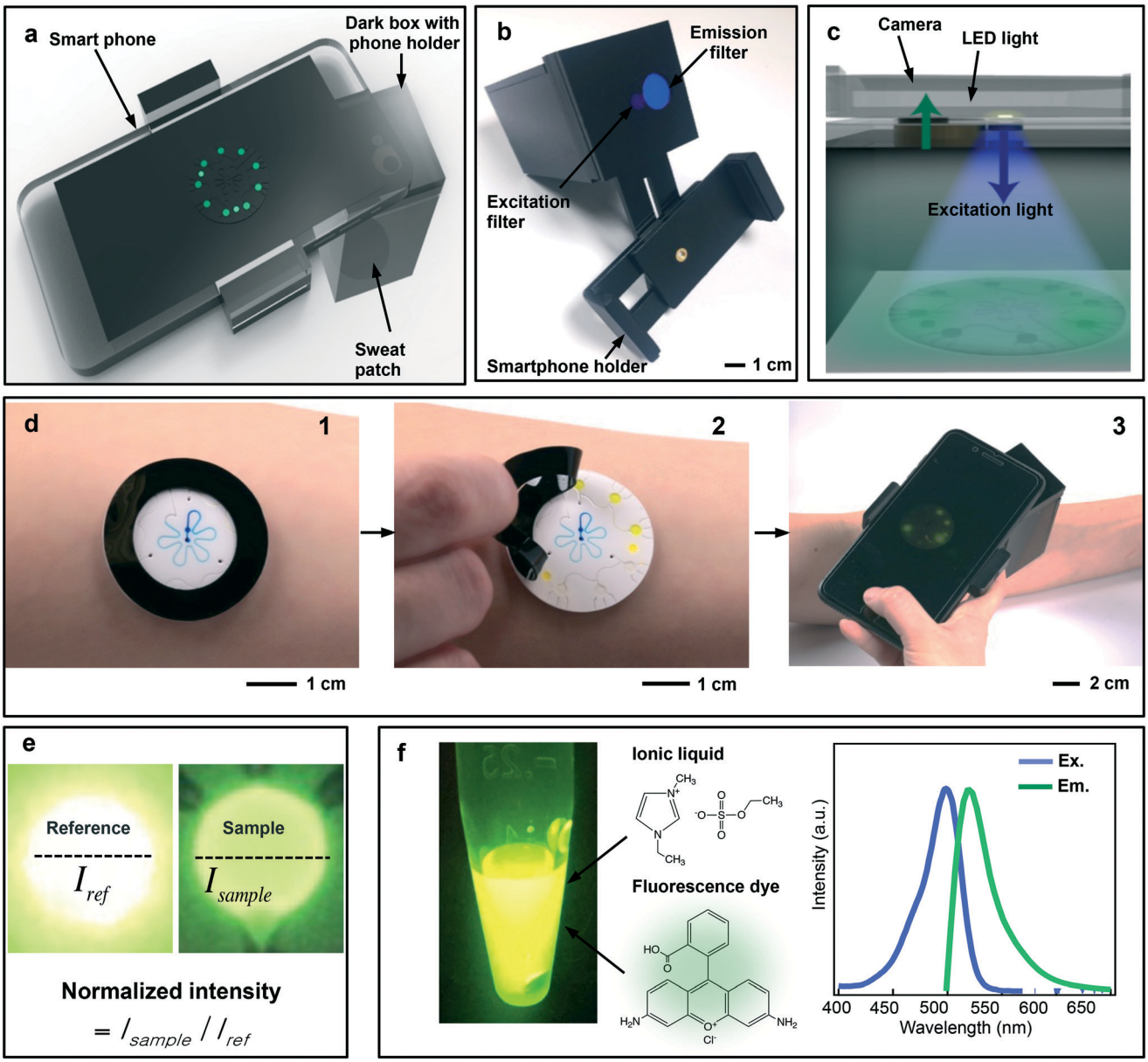

Fig. 2 Summary of key design aspects of a smartphone-based fluorometric imaging module. (a) Image of the overall concept of a fluorescence-imaging system based on a smartphone and an optics module. (b) Image of the optics module, consisting of a dark box with excitation/emission filters. (c) Image of the system, including a smartphone and optical filters. (d) Procedure for performing a fluorometric assay: 1. collecting sweat using a skin-interfaced microfluidic device 2. peeling away the black shield 3. capturing a photo of the device using a smartphone interfaced to the device with the optics module. (e) Method of fluorescence calibration. (f) Fluorescence reference material consisting of an ionic liquid and a fluorescence dye.

on an ordinary smartphone (Fig. 2b). The filters allow use of the LED flash as a source of excitation light and the imager as a detector of the resulting fluorescence (Fig. 2c). Specifically, a blue transparent film passes a narrow range of wavelengths (451 ± 35 nm) (Fig. S2a†) from the LED (Fig. S2b†) to excite the fluorescent probes (excitation wavelength of 400–530 nm, Fig. S3; (Fig. S4)†). A colored piece of glass blocks wavelengths below 515 nm, to allow measurement of excited fluorescence signals without interference from the excitation light.

Fig. 2d shows a sequence of images that detail the progression of sweat through the device. Sweat excreted from the skin first enters through the inlets and perfuses into the flower-shaped channel structures (Fig. 2d, left). Filling structure serves as an indication of filling of the three assay reservoirs because the volume is equal to that of the assay reservoirs, and the collection zones have similar sizes. At this stage, the user can remove the black film over the fluorescent reservoirs (Fig. 2d, middle) to capture fluorescent images of the microreservoir regions (Fig. 2d, right) using the smartphone and optical module.

Fluorescent signals from each microreservoir correlate quantitatively to the concentration of the target analyte (*i.e.* chloride, zinc, and sodium). Calibration involves first analyzing the intensity from the images (Image J software, NIH, USA) of each reservoir and normalizing these results by the intensity of the reference region (Fig. 2e). The reference consists of a stable fluorescence dye (Rhodamine chloride 110) dissolved in an ionic liquid to prevent evaporation.[35] Rhodamine chloride has an excitation wavelength comparable to that of the fluoroprobes studied here (Fig. 2f).[36]

Fluorescence quantification for sweat chloride, zinc, and sodium sensing

Different fluorescence probes spotted in each reservoir react with chloride, sodium, or zinc with high selectivity. Fig. 3a shows the assay microreservoirs for chloride, sodium, and

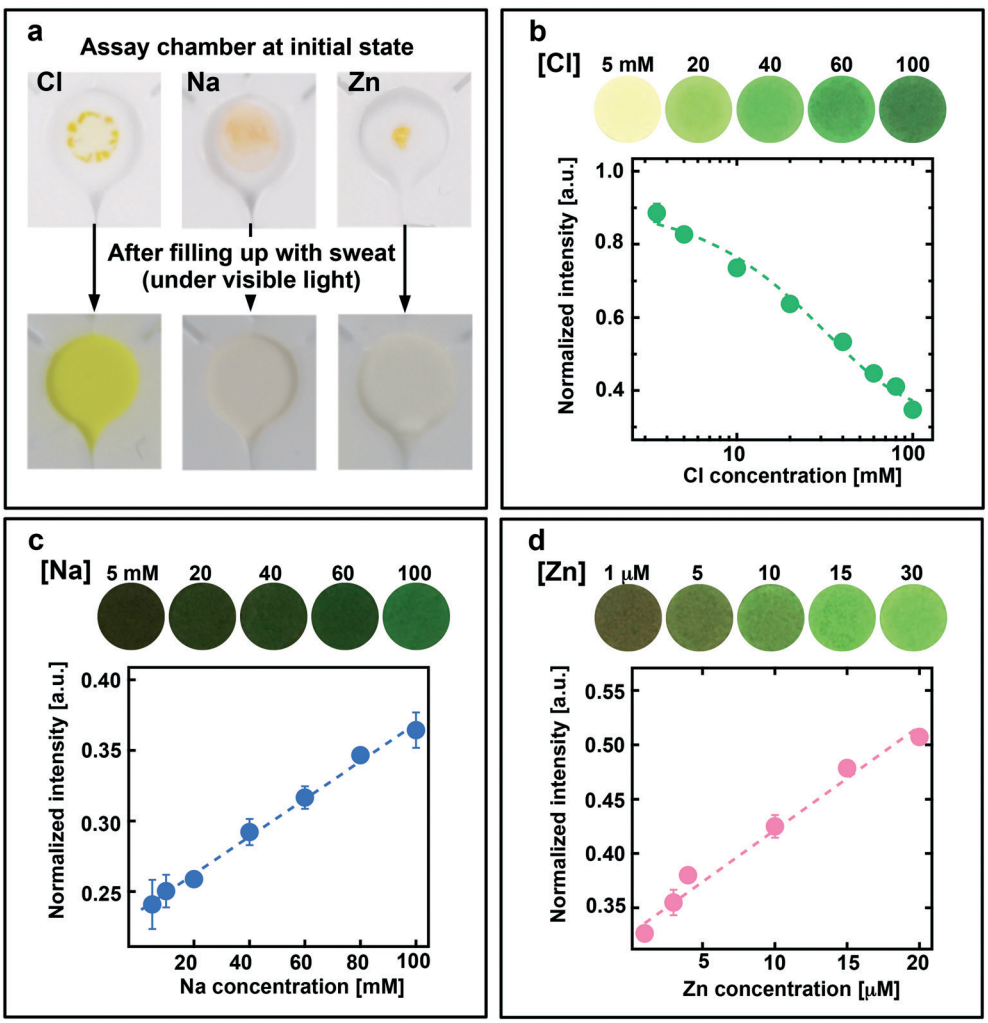

Fig. 3 Fluorescence images of chloride, zinc, and sodium assays and the dependence of the fluorescence intensity on concentration. (a) Image of the microreservoirs for the assays before (upper) and after (lower) filling with sweat collected under visible light illumination. Changes of the fluorescence and its normalized intensity at various concentrations of (b) chloride, (c) sodium, and (d) zinc.

zinc before and after filling with sweat. Fig. 3(b–d) summarizes smartphone images for a range of concentrations upon reaction in artificial sweat at pH 6. The graphs below the images show the dependence of the normalized intensity on the concentrations.

For chloride, the fluorescence intensity decreases exponentially with increasing chloride concentration in the range from 5 mM to 100 mM (Fig. 3b), which spans the normal range for sweat (~20–60 mM).[37] Here, the lucigenin fluorescent probes (λ_{ex} = 428 nm; λ_{em} = 511 nm, Fig. S3 and S4a†) react with chloride in a manner that quenches its fluorescence *via* a collisional mechanism.[38,39] The intensity of the fluorescence from the sodium probe, a crown ether derivative (λ_{ex} = 493 nm; λ_{em} = 515 nm, Fig. S3 and S4b†) increases linearly with sodium concentration upon binding of Na^+ (Fig. 3c).[40,41] Although the fluorescence signal is extremely low for

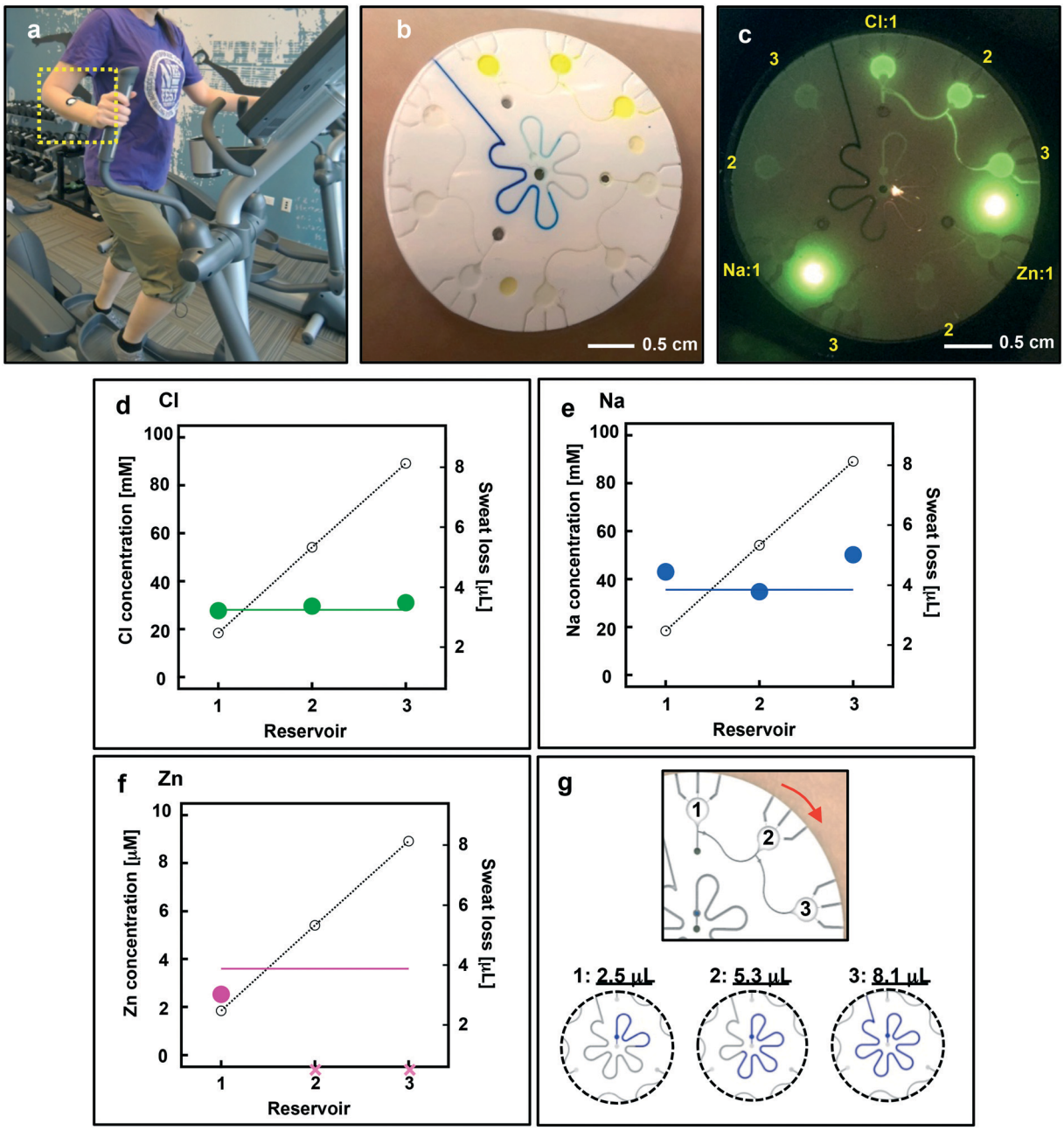

Fig. 4 Human trials. (a) Photograph of a subject wearing a microfluidic device during testing. Images of the device without the black shield after sweat collection under (b) visible light and (c) blue light emitted by a smartphone. (d) Calculated concentrations of sweat (d) chloride (green closed circles), (e) sodium (blue closed circles), and (f) zinc (pink closed circles), along with the estimated sweat loss (black dotted lines). The solid green, blue, and pink lines indicate the concentrations measured by ion chromatography for chloride, ICP-MS for zinc, and atomic absorption spectrometry for sodium. (g) Changes of estimated sweat loss as a function of extent of filling of the microreservoirs and the center microchannel structure.

concentrations below 20 mM, the intensity can be easily measured and shows a linear dependence on concentration across the normal range for sweat (~20–60 mM).[37] For zinc, the fluorescence intensity increases linearly with concentration over the range of 1 to 20 μM upon binding between the zinc probe (λ_{ex} = 490 nm; λ_{em} = 519 nm, Fig. S3†) and Zn^{2+} (Fig. 3d) which aligns with the physiological range (1.4–27 μM).[42,43] Taken together, the fluorescence intensities strongly correlate with the concentration of each target analyte with high reproducibility. These results suggest that fluorescent intensities in a microfluidic wearable sensor captured with a smartphone can be used to determine sweat chloride, sodium, and zinc with high accuracy (Fig. S5†).

Field studies

The studies involved microfluidic devices mounted on the right upper arms of healthy volunteers. Each ran on an elliptical trainer with a setting of middle strength load under controlled environmental conditions (23 °C at 50% relative humidity) (Fig. 4a). In these cases, the flower-shaped microchannel typically fill within 20 min after initiation of exercise. At the same time, the microreservoirs also completely fill, as confirmed by peeling off the black PDMS film (Fig. 4b). Rise in the rate of sweating to reach a steady state value occurs over the first ~10 min after the start of exercise. The lag/time for chronological sweat sampling in each of three reservoirs can therefore be estimated to be approximately 13, 16, and 20 min based on a well defined sweat rate (0.8 μL min^{-1}) calculated from the sweat sampling time (Fig. S6†). The sweat rate is comparable to results reported previously.[15] Capturing an image of the device using the smartphone and optics module yields fluorescence data for the probes for chloride, sodium, and zinc (Fig. 4c). After the exercise, approximately 100 μL of sweat was collected using a pipette on the left upper arm for subsequent analysis using ion chromatography, atomic absorption, and inductively coupled plasma mass spectrometry (ICP-MS) methods, respectively.

Fig. 4(d–f) shows chloride (28–31 mM), zinc (~2.5 μM), and sodium (35–50 mM) concentrations measured at each microreservoir following a workout routine. The concentrations are within the normal range and comparable to values determined using conventional ion chromatography for chloride (28 mM), ICP-MS for zinc (3.6 μM), and atomic absorption for sodium (36 mM). Fig. 4g shows time-sequential changes at the microreservoirs and the center channel. The concentrations of sodium in each reservoir tend to be higher than those of chloride. The trend is compatible with the reported results for normal subjects.[44] For zinc, the concentration at the first reservoir (~2.5 μM) is consistent with the reported physiological range (1.4 and 27 μM).[41,42] Zinc could not, however, be detected in the other reservoirs due to low fluorescence intensities. Improvements in the detection sensitivity are needed to allow measurements of zinc concentration in this case. The result suggests that the zinc concentration can change significantly during a workout.

Conclusions

The wearable fluorometric microfluidic platform and smartphone optics module introduced here establish a practical basis for point-of-care fluorescent-based sweat analysis. Measurements of chloride, sodium, and zinc concentrations in human exercise studies demonstrate some specific capabilities for sweat biomarker analysis, with validation against standard diagnostic instruments. These findings provide capabilities that extend and complement those of colorimetric schemes reported previously in skin-interfaced microfluidic systems and those of smartphone-based analyzing schemes for on-skin diagnostic systems.[45,46] The ease of use and the low-cost nature of these platforms could enable broad distribution across a wide assortment of chemical and immunoassay biomarker targets in sweat.

Experimental setup

The wearable sweat-analysis system introduced here consists of a thin, soft microfluidic device (Fig. 1) and a smartphone-based optics module (Fig. 2) for detecting fluorescence signals from chemical probes that interact with sweat, *in situ*. The fluidic device has micro-channels, microreservoirs and passive valves patterned in an elastomeric substrate (polydimethylsiloxane (PDMS), Sylgard 184; Dow Corning, MI, USA). The micropatterns define paths for the microchannels, allowing the device to capture and store microliter quantities of sweat for analysis of sweat loss and of chloride, sodium and zinc concentrations with fluorescence probes. The fluorescence imaging system includes a smartphone and optics module designed to capture fluorescent images of the microreservoirs.

Fabrication of the microfluidic system. The fabrication relied on soft lithographic techniques using patterned silicon molds. The first step involved laser etching of photomasks with patterns corresponding to the desired microchannel geometry. Spin casting (at 2000 rpm) photoresist (KMPR 1010; Microchem Inc., MA, USA) on a 4″ silicon wafer followed by baking at 110° C for 5 min on a hot plate defined a thin film for photopatterning (~15 μm in thickness). Next, passing UV light through the photomask placed on this coated wafer patterned the exposure of the resist. Immersing the silicon wafer in developer (AZ917 MIF; Integrated Micro Materials, TX, USA) removed the unexposed regions. Subsequently, deep reactive ion etching (STS Pegasus ICP-DRIE; SPTS Technologies Ltd., Newport, UK) created 400 μm deep trenches in the exposed silicon. Finally, spin coating a layer of poly(methyl methacrylate) (PMMA; Microchem Inc., MA, USA) on the silicon mold and baking at 180 °C for 10 min primed the mold to facilitate release of PDMS cast and cured on top.

Fabrication of microfluidic sweat device. The microfluidic devices consisted of five assembled layers: a light-shielding black film, a cover film, fluorometric assays, a microfluidic

substrate, and a skin-adhesive membrane (Fig. 1a). Fabricating this stack began with spin-casting a white silicone material (Silc Pig; Smooth-on, Inc., PA, USA) mixed at a ratio of 10 : 1 : 1 (base : curing agent : white silicone) on the silicon mold at 200 rpm, and then curing at 150 °C for 30 min. This baking process yielded a 1 mm thick, white microfluidic channel layer. Mechanical punches defined the inlet holes for collecting sweat and the exterior boundaries of the device. A transparent mixture of PDMS in a ratio of 10 : 1 (base : curing agent) spin cast on a PMMA-coated bare wafer at 300 rpm and cured at 150 °C for 30 min formed a uniform cover layer. Bonding the cover film to the microfluidic layer occurred after placing fluorometric assays in the wells. This bonding step formed the microfluidic channel pathways and microreservoir compartments. A small amount of PDMS (10 : 1) applied on the cover film before adding the channel layer, and then curing this material at 40 °C for 1 h defined an adhesive to ensure strong bonding without damage to the assay reagents. A black silicone formulation (Silc Pig; Smooth-on, Inc., PA, USA) mixed at a ratio of 10 : 1 : 1 (base : curing agent : black silicone) defined the light shielding layer. Spin coating at 300 rpm and curing at 150 °C for 30 min yielded a uniformly black elastic film. The black cover film laminates on top of the stack without any adhesives to yield a detachable and reusable light shielding layer. A CO_2 laser (Universal Laser Systems, AZ, USA) cut a double-sided skin adhesive membrane (PC2723U; ScapaHealthcare, CT, USA) into a round shape with defined openings. The adhesive membrane aligns with the inlet holes in the microfluidic PDMS substrate and bonds to its bottom surface. Plasma treating the microfluidic layer with a corona generator (Electro-Technic Products, IL, USA) created a hydrophilic PDMS surface to allow strong, irreversible bonding of the skin adhesive to the PDMS microfluidic substrate.

The chloride fluorometric assay consisted of 2 mg of lucigenin (Sigma-Aldrich, MO, USA) dispersed in 1 mL of deionized water (MilliQ, 18.2 MΩ cm). The zinc fluorometric assay solution was prepared by adding 25 μL of zinc detector (Zinc Quantification Kit (Fluorometric), Abcam Inc., MA, USA) into 5 mL of the zinc assay buffer. Dissolving 1 mg of the sodium detector (CoroNa™ Green; molecular probes, OR, USA) in 100 mL of dimethyl sulfoxide (Sigma-Aldrich, MO, USA) yielded a concentrated solution. Dispersing 2.3 μL of the concentrated solution into 1 mL of deionized water yielded the sodium fluorometric assay solution at a concentration of 40 μM. Dropping 2 μL volumes of each assay solution onto the respective chambers of the microfluidic layer, and then drying at 35 °C for 1 h in a light-shielded environment yielded solid-state chloride, zinc, and sodium assays, respectively (Fig. 3a). Dissolving 0.4 mg of rhodamine 110 chloride (Sigma-Aldrich, MO, USA) in 2 mL of 1-ethyl-3-methylilimidazolium ethyl sulfate ionic liquid (Sigma-Aldrich, MO, USA) formed the reference solution. Drop casting 0.5 μL of the ionic liquid dye into the chambers designed for the reference fluorometric dye completed the process.

Fabrication of a smartphone-based fluorescence imaging module. The imaging module consisted of an assembly of black acrylic pieces (McMaster-Carr, IL, USA), excitation (Scotchcal™ graphic film, 3632-87; 3M, MN, USA) and emission filters (colored-glass alternative filter, 5CGA-515, Newport Co., CA, USA), and a commercial smartphone fixture (Lotus Tech, Wembley, UK) to create the proper optical environment for fluorometric imaging (Fig. 2c). A CO_2 laser cut an acrylic black board with 3.18 mm into eight pieces. Gluing the four black plates together formed a square shaped box. Placing square plates with holes for excitation and emission filters on top defined the light-shielding box. The excitation and emission filters were fixed to the holes of the plate. The box was attached to the smartphone holder by a long rectangular acrylic piece with a screw. For alignment of the sweat patch, a square plate with a hole with a size equivalent to that of the patch was placed on the bottom of the box. The module serves to maintain a repeatable distance (8 cm) and angle (0°) between the camera and the microfluidic device. Placing pieces of black paper on the surface of the plates inside the box prevented light reflection. All fluorescence images were captured with a smartphone, iPhone 6 Plus (Apple Inc., CA, USA).

Imaging calibration tests. Calibration of the fluorescence system was performed before human trials using artificial sweat containing 22 mM urea (Sigma-Aldrich, MO, USA), 5.5 mM lactate acid, 3 mM NH^{4+} (NH_4Cl, Sigma-Aldrich, MO, USA), 0.4 mM Ca^{2+} ($CaCl_2$, Sigma-Aldrich, MO, USA), 50 μM Mg^{2+} ($MgCl_2$, Sigma-Aldrich, MO, USA), 25 μM uric acid (Sigma-Aldrich, MO, USA), and 0.1 mM glucose (Sigma-Aldrich, MO, USA) with varying chloride concentrations (5–100 mM), sodium concentrations (5–100 mM), and zinc concentrations (1–30 μM).[23] The zinc standard solution contained sodium and chloride with fixed concentrations of 20 mM. All of the solutions were equilibrated to pH 6 using KOH buffer (Sigma-Aldrich, MO, USA). The standard solutions were manually spotted in the microreservoirs of sweat microfluidic device using a micropipette. Capturing fluorescent images of the microreservoirs across different concentrations of test solutions, yielded concentration collaboration curves for each target analyte.

Conflicts of interest

There are no conflicts to declare.

Acknowledgements

This research was funded by the Air Force Research Laboratory (AFRL) Human Signatures Branch through Core funds provided to Northwestern University under contract FA8650-14-D-6516. This work utilized Northwestern University Micro/Nano Fabrication Facility (NUFAB), which is partially supported by Soft and Hybrid Nanotechnology Experimental (SHyNE) Resource (NSF ECCS-1542205), the Materials Research Science and Engineering Center (DMR-1720139), the

State of Illinois, and Northwestern University. This work (author Y. S.) was also partially supported by JSPS KAKENHI Grant JP16K21604.

References

1 K. Sato, *Rev. Physiol., Biochem. Pharmacol.*, 1977, **79**, 51–131.
2 K. Sato, W. H. Kang, K. Saga and K. T. Sato, *J. Am. Acad. Dermatol.*, 1989, **20**, 537–563.
3 T. Ohhashi, M. Sakaguchi and T. Tsuda, *Physiol. Meas.*, 1998, **19**, 449–461.
4 M. Shibasaki, T. E. Wilson and C. G. Crandall, *J. Appl. Physiol.*, 2006, **100**, 1692–1701.
5 N. A. Taylor and C. A. Machado-Moreira, *Extrem. Physiol. Med.*, 2013, **2**, 4.
6 C. J. Harvey, R. F. Lebouf and A. B. Stefaniak, *Toxicol. In Vitro*, 2010, **24**, 1790–1796.
7 Z. Sonner, E. Wilder, J. Heilenfeld, G. Kasting, F. Beyette, D. Swaile, F. Scherman, J. Joyce, J. Hagen, N. Kelley-Loungnane and R. Naik, *Biomicrofluidics*, 2015, **9**, 031301.
8 H. M. Emrich, E. Stoll, B. Friolet, J. P. Colombo, R. Richterich and E. Rossi, *Pediatr. Res.*, 1968, **2**, 464–478.
9 A. Mena-Bravo and M. D. Luque de Castro, *J. Pharm. Biomed. Anal.*, 2014, **90**, 139–147.
10 M. Calderon-Santiago, F. Priego-Capote, N. Trurck, X. Robin, B. Jurado-Gamez, J. C. Sanchez and M. D. Lunque de Castro, *Anal. Bioanal. Chem.*, 2015, **407**, 5381–5392.
11 K. Dolan, D. Rouen and J. Kimber, *Drug Alcohol Rev.*, 2009, **23**, 213–217.
12 S. Coyle, *et al.*, *IEEE Trans. Inf. Technol. Biomed.*, 2010, **14**, 364–370.
13 P. Wei, B. Morey, T. Dyson, N. McMahon, Y. Hsu, S. Gazman, L. Klinker, B. Ives, K. Dowling and C. Rafferty, *Proc. IEEE Sens*, Baltimore, MD, USA, 2013, vol. 32.
14 J. Heikenfeld, *et al.*, *Lab Chip*, 2018, **18**, 217–248.
15 J. Choi, R. Ghaffari, L. B. Baker and J. A. Rogers, *Sci. Adv.*, 2018, **4**, eaar3921.
16 D. P. Rose, M. E. Ratterman, D. K. Griffin, L. Hou, N. K. Loughnane, R. R. Nail, J. A. Hagen, I. Papautsky and J. C. Heilenfeld, *IEEE Trans. Biomed. Eng.*, 2015, **62**, 1457–1465.
17 S. Emaminejad, *et al.*, *Proc. Natl. Acad. Sci. U. S. A.*, 2017, **114**, 4625–4630.
18 R. Peng, *et al.*, *Lab Chip*, 2016, **16**, 4415–4423.
19 A. Koh, *et al.*, *Sci. Transl. Med.*, 2016, **8**, 366ra165.
20 J. Choi, D. Kang, S. Han, S. B. Kim and J. A. Rogers, *Adv. Healthcare Mater.*, 2017, **6**, 1601355.
21 S. B. Kim, *et al.*, *Small*, 2018, **14**, 1703334.
22 A. J. Bandodkar, W. Jia and J. Wang, *Electroanalysis*, 2015, **27**, 562–572.
23 W. Gao, *et al.*, *Nature*, 2016, **529**, 509–514.
24 H. Lee, *et al.*, *Sci. Adv.*, 2017, **3**, e1601314.
25 V. Oncescu, D. O'Dell and D. Erickson, *Lab Chip*, 2013, **13**, 3232–3238.
26 D. Zhang and Q. Liu, *Biosens. Bioelectron.*, 2016, **75**, 273–284.
27 A. Roda, M. Guardigli, D. Calabria, M. M. Calabretta, L. Cevenini and E. Michelini, *Anal. Chem.*, 2014, **139**, 6494–6501.
28 A. Roda, E. Michelini, L. Cevenini, D. Calabria, M. M. Calabretta and P. Simoni, *Anal. Chem.*, 2014, **86**, 7299–7304.
29 Q. Wei, *et al.*, *ACS Nano*, 2013, **7**, 9147–9155.
30 J. Chi, B. Gao, M. Sun, F. Zhang, E. Su, H. Liu and Z. Gu, *Anal. Chem.*, 2017, **89**, 7727–7733.
31 A. Cordova and F. J. Navasa, *Ann. Nutr. Metab.*, 1998, **42**, 274–282.
32 J. Choi, *et al.*, *Lab Chip*, 2017, **17**, 2572–2580.
33 D. Armani, C. Liu and N. Aluru, *MEMS '99; 12th IEEE International Conference*, 17–21 Jan, 1999, pp. 222–227.
34 D. Fuard, *et al.*, *Microelectron. Eng.*, 2008, **85**, 1283–1293.
35 T. Kan, H. Aoki, N. B. Khiem, K. Mastumoto and I. Shimoyama, *Sensors*, 2013, **13**, 4138–4145.
36 M. Beija, C. A. M. Afonso and J. M. G. Martinho, *Chem. Soc. Rev.*, 2009, **38**, 2410–2433.
37 M. Patterson, S. D. R. Galloway and M. A. Nimmo, *Exp. Physiol.*, 2000, **85**, 869–875.
38 C. Huber, C. Krause, T. Werner and O. S. Wolfbeis, *Mikrochim. Acta*, 2003, **142**, 245–253.
39 A. Graefe, *et al.*, *Anal. Chem.*, 2008, **80**, 6526–6531.
40 S. D. Meier, Y. Kovalchuk and C. R. Rose, *J. Neurosci. Methods*, 2006, **155**, 251–259.
41 R. W. Sabnis, *Handbook of Biological Dyes and Stains: Synthesis and Industrial Applications*, Wiley, 2010.
42 J. Kim, *et al.*, *Electrochem. Commun.*, 2015, **51**, 41–45.
43 K. C. DeRuisseau, S. N. Cheuvront, E. M. Haymes and R. G. Sharp, *Int. J. Sport Nutr. Exercise Metab.*, 2002, **12**, 428–437.
44 S. K. Hall, D. E. Stableforth and A. Green, *Ann. Clin. Biochem.*, 1990, **27**, 318–320.
45 N. MacKinnon, F. Vasefi, N. Booth and D. L. Farkas, *Proc. of SPIE*, 2016, vol. 9711, p. 971117.
46 A. Sahoo, A. Wahi and A. Das, *J. Pediat. Proc. of SPIE*, 2018, vol. 10485, DOI: 10.1117/12.2289857.

